Bioconjugate Chemistry

Article

pubs.acs.org/bc

Design, Preparation, and Characterization of PNA-Based Hybridization Probes for Affibody-Molecule-Mediated Pretargeting

Kristina Westerlund,[†] Hadis Honarvar,[‡] Vladimir Tolmachev,[‡] and Amelie Eriksson Karlström*[,†]

[†]School of Biotechnology, Division of Protein Technology, KTH Royal Institute of Technology, 106 91 Stockholm, Sweden

[‡]Department of Immunology, Genetics and Pathology, Uppsala University, 751 05 Uppsala, Sweden

ABSTRACT: In radioimmunotherapy, the contrast between tumor and normal tissue can be improved by using a pretargeting strategy with a primary targeting agent, which is conjugated to a recognition tag, and a secondary radiolabeled molecule binding specifically to the recognition tag. The secondary molecule is injected after the targeting agent has accumulated in the tumor and is designed to have a favorable biodistribution profile, with fast clearance from blood and low uptake in normal tissues. In this study, we have designed and evaluated two complementary peptide nucleic acid (PNA)-based probes for specific and high-affinity association in vivo. An anti-HER2 Affibody−PNA chimera, $Z_{HER2:342}$−SR−*HP1*, was produced by a semisynthetic approach using sortase A catalyzed ligation of a recombinantly produced Affibody molecule to a PNA-based *HP1*-probe assembled using solid-phase chemistry. A complementary *HP2* probe carrying a DOTA chelator and a tyrosine for dual radiolabeling was prepared by solid-phase synthesis. Circular dichroism (CD) spectroscopy and UV thermal melts showed that the probes can hybridize to form a structured duplex with a very high melting temperature (T_m), both in *HP1*:*HP2* and in $Z_{HER2:342}$−SR−*HP1*:*HP2* (T_m = 86−88 °C), and the high binding affinity between $Z_{HER2:342}$−SR−*HP1* and *HP2* was confirmed in a surface plasmon resonance (SPR)-based binding study. Following a moderately fast association (1.7×10^5 M^{-1} s^{-1}), the dissociation of the probes was extremely slow and <5% dissociation was observed after 17 h. The equilibrium dissociation constant (K_D) for $Z_{HER2:342}$−SR−*HP1*:*HP2* binding to HER2 was estimated by SPR to be 212 pM, suggesting that the conjugation to PNA does not impair Affibody binding to HER2. The biodistribution profiles of ^{111}In- and ^{125}I-labeled *HP2* were measured in NMRI mice, showing very fast blood clearance rates and low accumulation of radioactivity in kidneys and other organs. The measured radioactivity in blood was 0.63 ± 0.15 and 0.41 ± 0.15%ID/g for ^{125}I- and ^{111}In-*HP2*, respectively, at 1 h p.i., and at 4 h p.i., the kidney accumulation of radioactivity was 0.17 ± 0.04%ID/g for ^{125}I-*HP2* and 3.83 ± 0.39%ID/g for ^{111}In-*HP2*. Taken together, the results suggest that a PNA-based system has suitable biophysical and in vivo properties and is a promising approach for pretargeting of Affibody molecules.

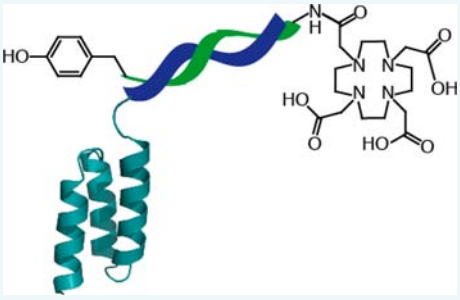

INTRODUCTION

Radioimmunotherapy (RIT) is a type of targeted therapy based on radiolabeled monoclonal antibodies binding to disease-associated molecular targets. RIT has been approved for treatment of non-Hodgkin B-cell lymphoma and is being explored for other cancers.[1,2] In contrast to lymphomas, solid tumors are more radioresistant. The large size of antibodies leads to poor extravasation and tumor penetration, which in combination with the long half-life in circulation, leads to significant exposure to other tissues, including the very radiosensitive bone marrow. This prevents delivery of sufficiently absorbed dose to tumors without overirradiating critical normal tissues.

An alternative to full-length antibodies is to use other targeting agents, such as antibody fragments, alternative scaffold proteins, or peptides. Using smaller targeting agents, better tumor penetration and more rapid clearance from nontumor tissue is expected. One example of an alternative scaffold protein is the Affibody molecule, which is a 7 kDa targeting protein that can be engineered to bind to tumor-associated targets such as HER2, EGFR, HER3, IGF-1R, and CAIX.[3−8] Affibody molecules have been extensively explored as targeting agents for molecular imaging of tumors and could also be attractive candidates for targeted radionuclide therapy, if labeled with residualizing radiometals such as ^{177}Lu, ^{212}Bi, ^{213}Bi, or ^{227}Th.[9] However, although Affibody molecules bind with high affinity to their respective targets and are rapidly cleared from blood, the renal clearance is accompanied by a high degree of reabsorption and retention of radioactivity in the kidney. Unfavorable biodistribution and unwanted uptake in different organs may thus complicate the use of both antibodies and alternative scaffold proteins as targeting agents in RIT.

One way to overcome these problems is to use a pretargeting system, in which the targeting agent and the radiolabel are injected separately, in a two-step procedure. In the first step, the primary targeting agent, which is conjugated to a recognition tag, is injected in the patient. Over time, the targeting agent will accumulate in the tumor and clear from

Received: May 21, 2015
Revised: June 18, 2015
Published: June 18, 2015

DOI: 10.1021/acs.bioconjchem.5b00292
Bioconjugate Chem. 2015, 26, 1724−1736

blood and nontumor tissue. In the second step, a secondary radiolabeled molecule binding specifically (covalently or noncovalently) to the recognition tag is injected and will bind to the targeting agent. Because the primary targeting agent is not radiolabeled, a higher dose can be injected to saturate the tumor without accompanying toxicity. The secondary radiolabeled molecule should be designed to have a favorable biodistribution profile, including fast clearance from blood and low uptake in normal tissues. A strong precondition for successful application of the pretargeting strategy for Affibody molecules is their slow internalization by malignant cells but rapid internalization upon reabsorption in kidneys.[9] Therefore, the recognition tags would remain exposed on the surface of cancer cells after clearance of primary agent but would be removed from the lumen of the proximal tubuli.

The concept of pretargeting was introduced previously in the 1980s, and several different types of pretargeting systems have been described in the literature.[10−12] One type of system relies on the noncovalent, high-affinity interaction between biotin and streptavidin/avidin.[13,14] However, the immunogenicity of streptavidin and avidin remains a major problem with this approach as well as the presence of endogenous biotin and biotinidases.[15−17] Another system is based on bispecific antibodies, with one part binding the tumor-associated target and the other part directed toward a radiolabeled hapten, such as indium complex of DTPA or EDTA.[18] Although the affinity between the antibody and the hapten is several orders of magnitude lower than the corresponding affinity between biotin and streptavidin, the concept has shown promising results in preclinical studies.[19] Drawbacks of this strategy include potential immunogenicity and the expensive production of the bispecific antibody construct. An elegant, recently explored strategy is based on bioorthogonal chemical reactions that proceed with high efficiency and are selective in vivo. The inverse-electron-demand Diels−Alder reaction between strained *trans*-cyclooctene (TCO) and electron-deficient tetrazine appears particularly promising, although there has been some concerns regarding deactivation of the TCO derivative by copper-containing serum proteins.[20−22] However, by optimization of the linker between TCO and the radionuclide chelator, the in vivo stability could be improved.[23,24]

Another strategy for pretargeting is based on complementary DNA oligonucleotides. This approach has the advantages of high affinity between the complementary strands and the option to fine-tune the binding affinity by changing the composition and length of the oligomers. To avoid degradation by nucleases, backbone-modified analogues can be used. One example are morpholino oligomers (MORFs), in which the DNA backbone composed of alternating phosphodiester and deoxyribose groups is replaced with a phosphorodiamidate morpholino backbone.[25−27] Peptide nucleic acid (PNA) is another class of synthetic DNA mimics, in which the native backbone has been exchanged for a pseudopeptide backbone. The PNA backbone is built up of repeating *N*-(2-aminoethyl) glycine units connected by amide bonds, and standard purine and pyrimidine nucleobases are connected to this scaffold through short, flexible carboxymethyl linkers.[28,29]

The aim of the present study was to develop a pretargeting system based on complementary PNA probes, for selective delivery of radionuclides to tumors using Affibody molecules as targeting agents. We can foresee many potential benefits of using PNA:PNA hybridization as the specific recognition mechanism in pretargeting applications. The highly flexible and charge-neutral PNA backbone permits the nucleobases to base-pair with complementary PNA sequences, obeying the Watson−Crick complementarity rules, and PNA:PNA duplexes show thermal stabilities that exceed those of native oligonucleotides duplexes.[30] Being neither a peptide nor a nucleic acid makes PNA resistant to both nuclease and protease degradation, and PNA molecules show excellent stability in human blood serum.[31] PNAs are nonimmunogenic, have low general toxicity in vivo, and show low cellular uptake in vivo because of the charge-neutrality of the scaffold.[32−36] PNA-based hybridization probes have previously been suggested for pretargeting applications, and early studies in mouse models demonstrated that ^{99m}Tc-labeled PNA strands could hybridize in vivo to complementary biotinylated PNA strands, conjugated to either streptavidin or streptavidin-coated polystyrene beads.[35,37] However, to the best of our knowledge, PNA pretargeting has not been demonstrated for specific targeting using antibodies or other selective targeting agents.

In this study, we describe the production of an anti-HER2 Affibody−PNA chimera, $Z_{HER2:342}$−SR−*HP1*, for tumor-specific delivery of the PNA-based *HP1* probe to HER2-expressing cells, and a complementary PNA-based effector probe, denoted *HP2*. An in vitro biophysical characterization of $Z_{HER2:342}$−SR−*HP1* and the *HP2*-probe was undertaken to evaluate the kinetics and affinity of the hybridization reaction between the PNA-based probes, and to investigate the binding of the Affibody−PNA chimera to the HER2 receptor. A fast blood clearance rate and low kidney accumulation of the effector probe is vital for our proposed pretargeting strategy. In this article, we evaluated the general biodistribution profile of both ^{111}In- and ^{125}I-labeled *HP2* in normal NMRI mice.

RESULTS AND DISCUSSION

Here, we describe the design and solid-phase assembly of two complementary 15-mer hybridization probes *HP1* and *HP2*. One of the probes, *HP1*, is designed to be covalently attached to an anti-HER2 Affibody molecule, to create an Affibody−PNA chimera capable of high-affinity binding to both the HER2 receptor and the complementary *HP2* effector probe. The PNA conjugation of the Affibody molecule should be irreversible and site-specific to produce a homogeneous chimera, and the conjugation site should be located away from the antigen-recognition site so that the binding affinity is not adversely affected by the labeling. Here, we turn to the bacterial transpeptidase sortase A to conjugate an Affibody molecule with *HP1*. The *HP2* effector probe carries both a DOTA chelator for radiometal complexing and a tyrosine for direct radioiodination and is designed to bind selectively, and with high-affinity, to the Affibody−PNA chimera in vivo or be eliminated through fast renal excretion.

Design and Synthesis of PNA Hybridization Probes. The hybridization probes *HP1* and *HP2* (Figure 1 and Table 1) were designed for high-affinity association in vivo via their 15-mer PNA domains. Very high melting temperatures (in the 70−80 °C range) have been determined earlier for PNA:PNA duplexes of similar lengths and sequence compositions.[38] Partially self-complementary PNA sequences were specifically avoided in our probe design. Because of the inherent backbone flexibility of PNA, self-complementary PNA molecules can self-hybridize and form very stable stem−loop structures.[39] If stable self-hybridization must be disrupted before duplex formation, then this may have a detrimental effect on the hybridization

DOI: 10.1021/acs.bioconjchem.5b00292
Bioconjugate Chem. 2015, 26, 1724−1736

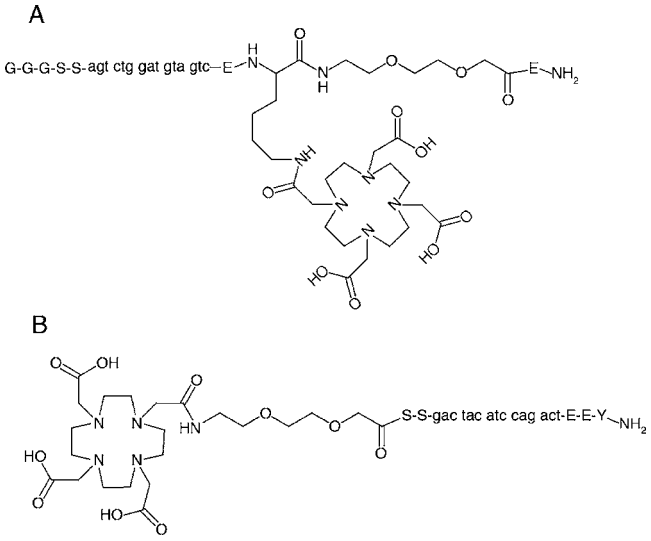

Figure 1. Hybridization probes (A) *HP1* and (B) *HP2*. Amino acids are denoted with upper case one-letter codes (G, E, K, S, and Y) and PNA monomers are given in lowercase letters (a, c, g, and t). The sequences are shown with the N-terminal residue on the left and the C-terminal residue on the right. Both probes have C-terminal amides.

efficiency. This is of special importance in an in vivo setting, in which our ability to change parameters (such as temperature, pH, or ionic strength) to influence the self-hybridization is severely limited.[40] The *HP1* probe has an N-terminal GGG tag for sortase A mediated ligation to an Affibody molecule and a DOTA chelator. DOTA was introduced to provide an opportunity to radiolabel the Affibody−PNA chimera with, for example, the gamma-emitting radionuclide ^{111}In or the positron-emitting radionuclide ^{68}Ga. At the preclinical stage and in clinical trials, radiolabeling would provide a convenient way for studying the pharmacokinetics of $Z_{HER2:342}$−SR−*HP1*. This can help to optimize the dosing of the Affibody−PNA chimera and the waiting period before administration of the radiolabeled secondary agent, *HP2*. In clinical situations, radiolabeled $Z_{HER2:342}$−SR−*HP1* might be used in pretreatment imaging in order to identify patient subsets most likely to benefit from pretargeted radionuclide therapy, i.e., patients with tumors avidly accumulating the Affibody−PNA chimera. Patients with low tumor uptake of radiolabeled $Z_{HER2:342}$−SR−*HP1* can be excluded from treatment and spared the adverse effects of an inefficient treatment. The effector probe, *HP2*, is dually functionalized for radiolabeling, with a DOTA chelator for radiometal complexing and a tyrosine for direct radioiodination. Direct radioiodination takes place under in situ oxidation of radioiodide in the presence of tyrosine. Treatment of radioiodide with a oxidant, e.g., chloramine-T (sodium chloro-(4-methylphenyl) sulfonylazanide), results in the formation of interhalogen iodine monochloride ICl, which dissociates with formation of electrophilic radioiodine.[41] Electrophilic radioiodine attacks highly activated phenolic rings of tyrosine residues resulting in iodotyrosine.[42] The triglycine motif in *HP1* and the DOTA chelator in *HP2* are placed at the N terminus of their respective probes. With this placement, the chelator and the Affibody molecule attachment sites are positioned as far apart as possible when the probes hybridize to form an antiparallel duplex. To ensure high water solubility, the purine content in the probes was kept below 60% (53% in *HP1* and 47% in *HP2*), and a maximum of three

Table 1. Sequences and Theoretical and Observed Molecular Weights of Probes, Proteins, and Conjugates

probes, proteins, and conjugates	sequence[a]	theoretical MW (Da)	observed MW (Da)
HP1	GGG-agt ctg gat gta gtc-EK(DOTA)-[AEEA]-E-NH_2	5396.4	5396.5
HP2	DOTA-[AEEA]-SS-gac tac atc cag act-EEY-NH_2	5157.8	5158.3
$Z_{HER2:342}$−SR−H_6	•VDNKFNKEMRNAYWEIALLPNLNNQQKRAFIRSLYDDPSQSANLLAEAKKLNDAQAPK•VDGSGSGSLPETGGHHHHHH	8729.6	8729.8
$Z_{HER2:342}$−SR−*HP1*	•VDNKFNKEMRNAYWEIALLPNLNNQQKRAFIRSLYDDPSQSANLLAEAKKLNDAQAPK•VDGSGSGSLPETGGG-agt ctg gat gta gtc-EK(DOTA)-[AEEA]-E-NH_2	13170.6	13171.3[b]

[a]Abbreviations: DOTA=1,4,7,10-tetraacacyclododecane-1,4,7,10-tetraacetic acid, [AEEA]=[2-(2-aminoethoxy)ethoxy]acetic acid. Amino acids are denoted with upper case one-letter codes and PNA monomers are given in lower case letters. The original $Z_{HER2:342}$ sequence is separated by bullets. [b]Dominant mass in the 4−30 kDa range

DOI: 10.1021/acs.bioconjchem.5b00292
Bioconjugate Chem. 2015, 26, 1724−1736

consecutive purines were introduced in the probes.[43] PNA oligonucleotides are commonly synthesized with lysines at the C terminus to enhance solubility.[44] This was avoided in our design because results obtained earlier on anti-HER2 Affibody molecules suggest an increased hepatic uptake in mice upon the introduction of positive charges.[45] Instead, to prevent self-aggregation and improve solubility, we introduced negative (glutamate) and polar (serine) amino acids and a hydrophilic, PEG-based linker at positions flanking the PNA hybridization domain. The introduction of the flexible linkers was also hypothesized to prevent steric hindrance between the hybridization domain and other functional parts of the probes. *HP1* (Scheme 1) and *HP2* were successfully assembled using manual solid-phase synthesis according to published procedures.[46] Crude probes were purified using reversed-phase HPLC, and the molecular weights of *HP1* and *HP2* were verified using electrospray mass spectrometry (Table 1).

Scheme 1. Synthesis of the *HP1* Hybridization Probe

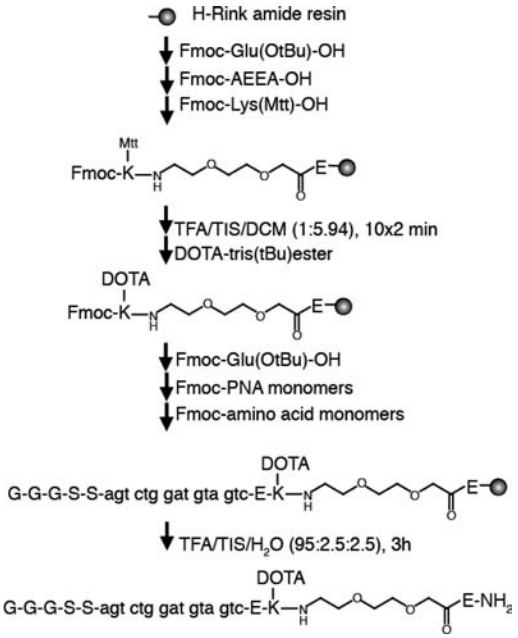

Production of the Affibody−PNA Chimera. $Z_{HER2:342}$−SR−H_6 was created by genetically fusing the amino acid sequence of the parental $Z_{HER2:342}$ molecule with a C-terminal peptide extension.[4] This extension contains a flexible $(GS)_3$ linker, an optimized sortase A recognition (SR) motif (LPETGG), and a His_6 affinity tag, which is later cleaved off in the sortase A catalyzed ligation.[47,48] The extension is added to make the anti-HER2 Affibody a substrate for sortase A mediated ligation. The recognition site, which is responsible for the picomolar affinity of the parental $Z_{HER2:342}$ Affibody molecule for HER2, is situated on helices 1 and 2 of the 3-helix Z scaffold.[49] By introducing the attachment site for the PNA-based probe at the C-terminal end of helix 3, we reduced the risk of sterical hindrance between the HER2 recognition site and the PNA-based hybridization domain. $Z_{HER2:342}$−SR−H_6 was expressed in *Escherichia coli* and purified using immobilized metal-affinity chromatography (IMAC). The protein was estimated to be >90% pure following IMAC purification, as judged by SDS-PAGE gel electrophoresis (data not shown). Electrospray mass spectrometry was used to confirm the identity of the protein (Table 1).

To efficiently produce the Affibody−PNA chimera, we turned to a semisynthetic approach. The recombinantly expressed anti-HER2 Affibody molecule, $Z_{HER2:342}$−SR−H_6, was enzymatically fused, using sortase A mediated ligation (SML), with an *HP1* probe assembled using solid-phase synthesis (Figure 2). Sortase A is a transpeptidase isolated from the bacterium *Staphylococcus aureus*, where the enzyme is responsible for anchoring substrate proteins to the cell wall.[50] Folded proteins carrying a C-terminal and solvent-exposed LPXTG-tag (in which X is any amino acid) are recognized as substrates by sortase A. The enzyme cleaves the Thr−Gly amide bond in the LPXTG tag, and then catalyzes the formation of a new peptide bond between the protein and an incoming fusion partner carrying an N-terminal oligoglycine motif. SML has in recent years become an important tool for bioconjugation and has been used for both N- and C-terminal labeling of proteins for a wide variety of applications.[51,52] The addition of the small LPXTG tag to the C terminus of recombinantly produced proteins is generally well-tolerated and rarely compromises the production and folding or the biological function of the expressed proteins. The potential fusion partner has to be functionalized with an N-terminal (oligo)glycine motif, but as long as the glycine motif is solvent-exposed, the identity of the fusion partner seems to be of little importance for an efficient conjugation reaction.[51] Sortase A has previously been used to site-specifically ligate fusion partners to $Z_{HER2:342}$, both to the N terminus (anthrax and diphtheria toxins) and the C terminus (NIR fluorescent dyes and introduction of an azide group for subsequent nanoparticle attachment). Importantly, the produced anti-HER2 Affibody conjugates all retained HER2-receptor-specific binding.[47,53] An active antisense PNA−peptide chimera has also previously been produced using SML, but we note that our $Z_{HER2:342}$−SR−*HP1* design has the reverse peptide-to-PNA order.[54] $Z_{HER2:342}$−SR−*HP1* was successfully prepared following the scheme outlined in Figure 2, and the identity of the Affibody−PNA chimera was confirmed using electrospray mass spectrometry (Table 1). HPLC chromatography indicated a ligation efficiency of ∼45% (on the basis of *HP1*) after a 24 h SML reaction (Figure 3A). Unreacted *HP1* from the final HPLC purification step was reused in another round of SML together with fresh $Z_{HER2:342}$−SR−H_6 to increase the total amount of Affibody−PNA chimera produced. The final purity of $Z_{HER2:342}$−SR−*HP1* (Figure 3B) and *HP2* (Figure 3C) was assessed using reversed-phase HPLC and estimated to be >90 and >95%, respectively.

Spectroscopic Characterization. The secondary structure of $Z_{HER2:342}$−SR−H_6 and $Z_{HER2:342}$−SR−*HP1* was investigated using circular dichroism (CD) spectroscopy. The obtained CD spectra (Figure 4A) display minima at around 222 nm, characteristic of proteins with high helical content. Spectra collected before and after thermal denaturation at 90 °C suggest that both samples regained at least 95% of the initial signal upon refolding (data not shown). CD spectroscopy was also used to study the secondary structure of the PNA-based hybridization probes. Unmodified PNA oligomers are achiral, but the introduction of C-terminal chiral amino acids can introduce a preferred helical handedness in the PNA oligomer and thus a CD signal.[38,55] *HP1* and *HP2* both display weak CD signals (Figure 4B), probably because of a high degree of backbone flexibility in their single-stranded states.[38] However, when hybridized in an antiparallel *HP1*:*HP2* duplex, a CD signal characteristic of a left-handed P helix is induced in the complex (Figure 4B).[38,55] The P helix is a form of helical

DOI: 10.1021/acs.bioconjchem.5b00292
Bioconjugate Chem. 2015, 26, 1724−1736

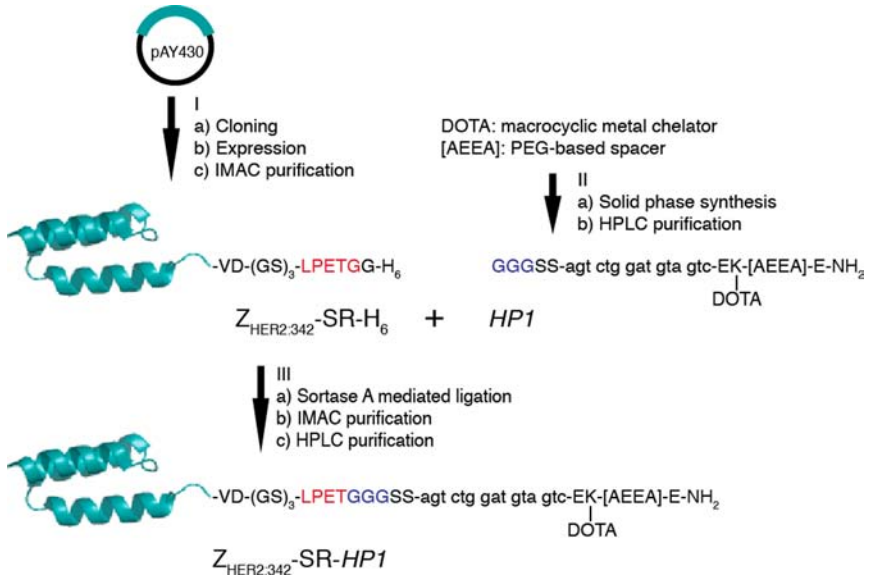

Figure 2. Preparation of the $Z_{HER2:342}$−SR−*HP1* chimera. Hybridization probe *HP1* was site-specifically attached to the HER2-specific $Z_{HER2:342}$ Affibody molecule via a sortase A mediated ligation. (I) The $Z_{HER2:342}$ Affibody molecule was recombinantly fused at the C terminus with a $(GS)_3$ linker, an optimized sortase A recognition sequence (here abbreviated SR) with the sequence LPETGG, and a His_6 affinity tag. $Z_{HER2:342}$−SR−H_6 was cloned and produced in *E. coli* and purified under native conditions using immobilized metal-affinity chromatography (IMAC). *HP1* contains a 15-mer PNA hybridization sequence, complementary to the PNA sequence in *HP2*, and carries a triglycyl sequence at the N terminus to make it a substrate for sortase A mediated ligation. (II) *HP1* was assembled using solid-phase Fmoc chemistry and purified on a semipreparative HPLC column. $Z_{HER2:342}$−SR−H_6 and *HP1* were mixed, and sortase A was added to catalyze the formation of $Z_{HER2:342}$−SR−*HP1* via a two-step transpeptidase reaction. (III) The fusion product was purified by sequential IMAC and HPLC steps.

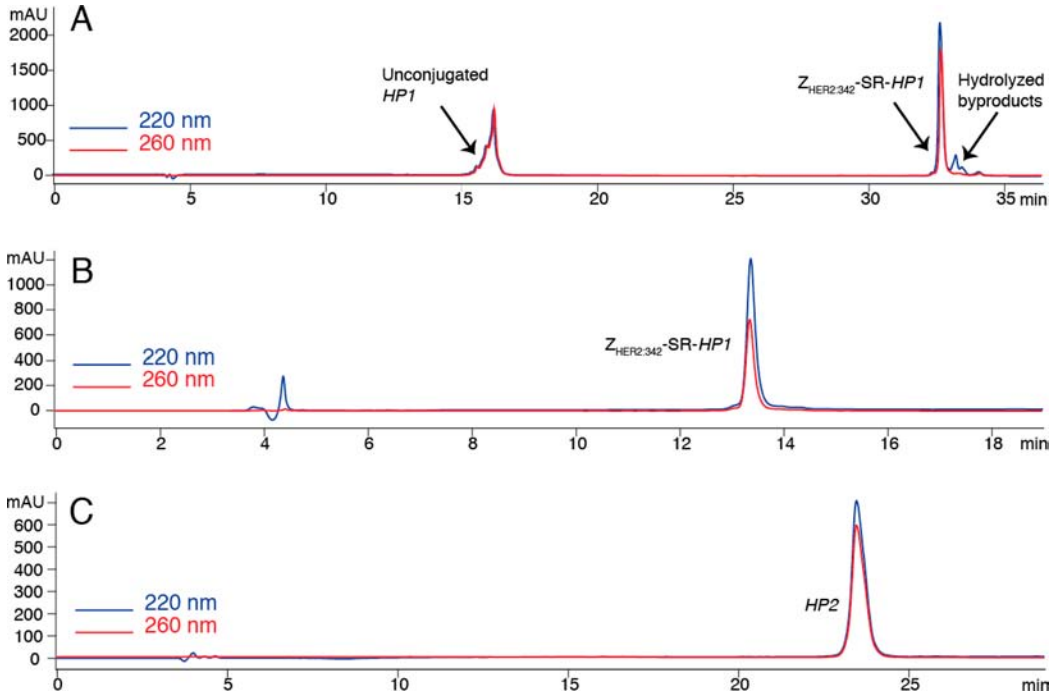

Figure 3. (A) Representative chromatogram from the final HPLC purification step (step IIIc in Figure 2) following the sortase A mediated ligation of *HP1* to $Z_{HER2:342}$−SR−H_6. More than 45% of the eluted *HP1* is present in $Z_{HER2:342}$−SR−*HP1*, as estimated by the absorbance at 260 nm. Excess $Z_{HER2:342}$−SR−H_6 was removed in the IMAC purification step (step IIIb in Figure 2) preceding this final purification step. RP-HPLC analysis showing the purity of (B) $Z_{HER2:342}$−SR−*HP1* and (C) *HP2*. $Z_{HER2:342}$−SR−*HP1* and *HP2* are more than 90 and 95% pure, respectively, as estimated by the absorbance at 220 nm.

structure, adopted by PNA:PNA duplexes. Compared to helical DNA duplexes, P helixes have a larger pitch, a wider and deeper major groove, and a narrower and shallower minor groove.[55] To investigate the structure of the *HP1*:*HP2* duplex in $Z_{HER2:342}$−SR−*HP1*:*HP2*, a CD difference spectrum was calculated by subtracting the CD spectrum of $Z_{HER2:342}$−SR−H_6 (Figure 4A) from the spectrum of $Z_{HER2:342}$−SR−*HP1*:*HP2* (Figure 4A). The calculated CD difference spectrum (Figure

DOI: 10.1021/acs.bioconjchem.5b00292
Bioconjugate Chem. 2015, 26, 1724−1736

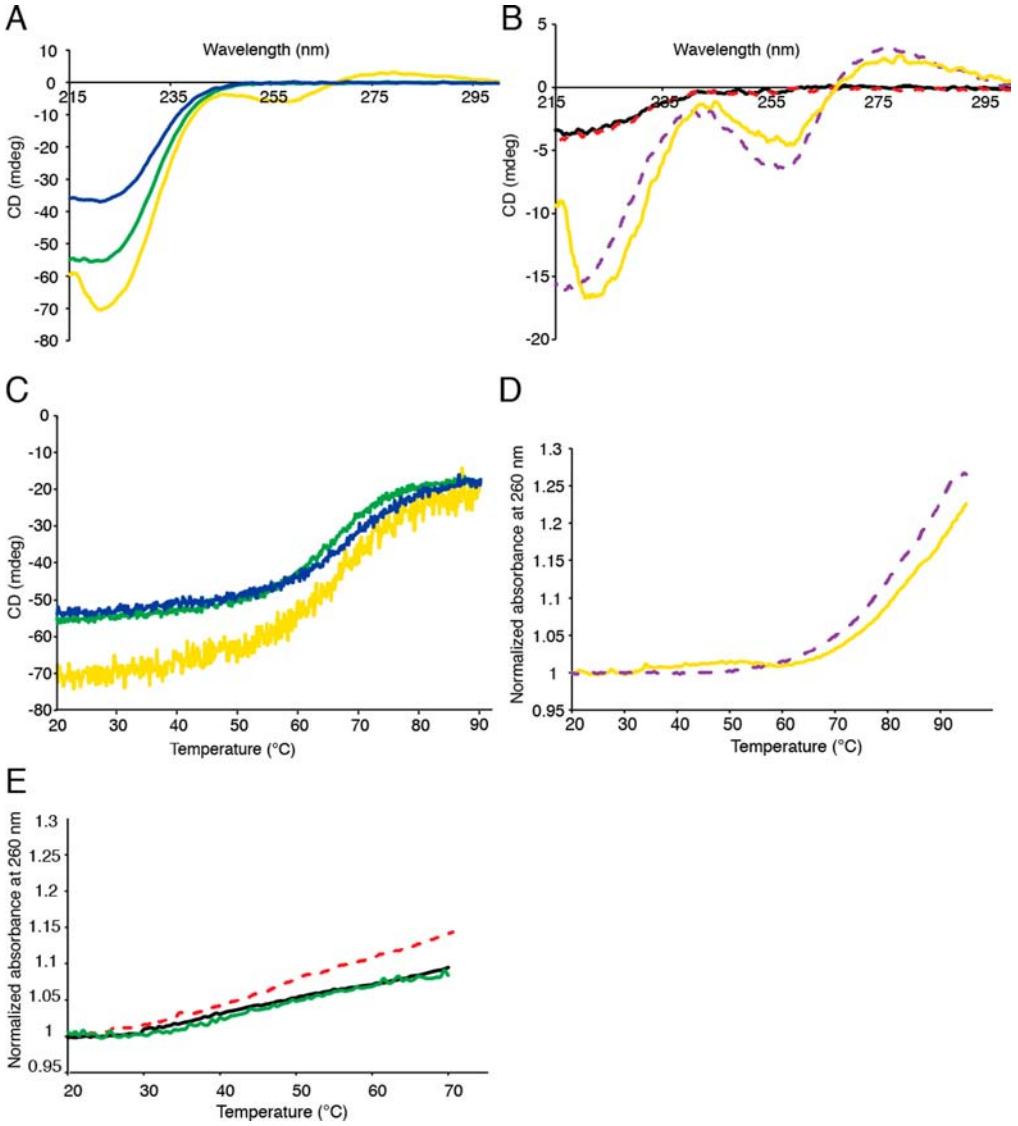

Figure 4. Spectroscopic characterization of proteins, hybridization probes, and chimeras. (A) Circular dichroism (CD) spectra of 33 μM $Z_{HER2:342}$−SR−H_6 (blue), 33 μM $Z_{HER2:342}$−SR−*HP1* (green), and 33 μM $Z_{HER2:342}$−SR−*HP1*:*HP2* (yellow). (B) CD spectra of 20 μM *HP1*:*HP2* (purple dashed line), 21 μM *HP1* (black solid line), and 20 μM *HP2* (red dashed line). A calculated CD difference spectrum (33 μM $Z_{HER2:342}$−SR−*HP1*:*HP2* − 33 μM $Z_{HER2:342}$−SR−H_6) is included for comparison (yellow line). All CD spectra in A and B were collected at 20 °C. (C) The loss of secondary structure as a function of temperature was followed by monitoring the CD intensity at 221 nm. $Z_{HER2:342}$−SR−H_6 (blue) and $Z_{HER2:342}$−SR−*HP1* (green) give rise to sigmoidal melting profiles indicative of cooperative unfolding. The loss of optical signal in $Z_{HER2:342}$−SR−*HP1*:*HP2* (yellow) is not expected to follow a simple two-state mechanism but is included for comparison. (D) UV melting curves of *HP1*:*HP2* (purple dashed line) and $Z_{HER2:342}$−SR−*HP1*:*HP2* (yellow line). (E) UV melting curves of *HP1* (black), *HP2* (red dashed line), and $Z_{HER2:342}$-SR−*HP1* (green). Concentration of monomers and duplexes in D and E are 5 μM. All spectra in Figure 4 were recorded in 20 mM potassium buffer with 100 mM KCl (pH 7.4).

4B) is very similar to the CD spectrum of the *HP1*:*HP2* complex, both in terms of amplitude and shape. This indicates that the *HP1*:*HP2* duplex has a similar secondary structure on its own and when *HP1* is covalently attached to the anti-HER2 Affibody molecule in $Z_{HER2:342}$−SR−*HP1*:*HP2*. The global stability of $Z_{HER2:342}$−SR−*HP1* and $Z_{HER2:342}$−SR−H_6 was studied by monitoring the CD intensity at 221 nm as a function of temperature between 20 and 90 °C (Figure 4C). The obtained melting temperatures of the two proteins are very similar, 68 and 66 °C for $Z_{HER2:342}$−SR−H_6 and $Z_{HER2:342}$−SR−*HP1*, respectively, and are in excellent agreement with the melting temperature (67 °C) determined earlier for the $Z_{HER2:342}$ parental molecule.[4] The CD signal at 221 nm as a function of temperature was also studied for $Z_{HER2:342}$−SR−*HP1*:*HP2* (Figure 4C). An apparent T_m of 67 °C can be fitted to the data, but the loss of signal from this complex is not expected to follow a simple two-state mechanism. An induced CD signal arising from a PNA:PNA duplex is sensitive to conformational changes in the duplex structure, and a complete loss of CD intensity often precedes thermally induced base dissociation (as measured in UV thermal melts).[38,55] This effect can be quite prominent, especially for longer PNA molecules. For example, a His-containing 15-mer PNA:PNA duplex was shown to have a T_m of 77 °C (midpoint transition temperature measured with UV) and a $T_{1/2}$ of 60 °C (midpoint transition temperature measured with CD).[38]

UV thermal melts were used to determine the melting temperature of the *HP1*:*HP2* duplex, alone and in $Z_{HER2:342}$−

DOI: 10.1021/acs.bioconjchem.5b00292
Bioconjugate Chem. 2015, 26, 1724−1736

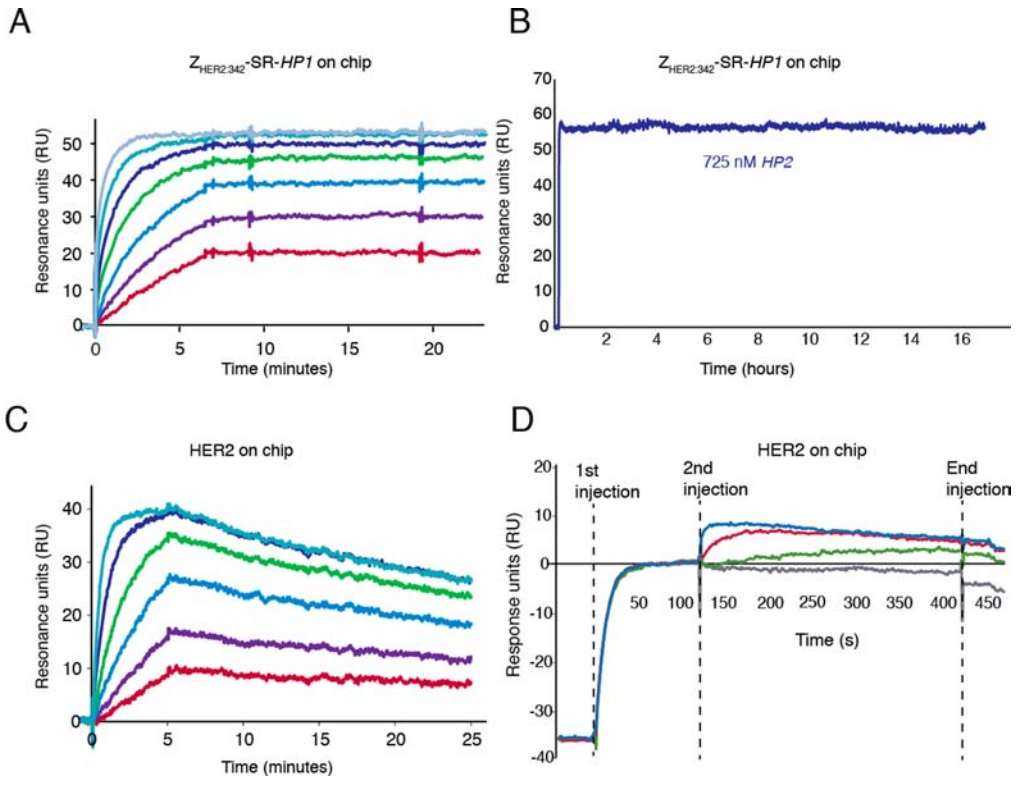

Figure 5. (A) Representative SPR sensorgrams of *HP2* binding to immobilized $Z_{HER2:342}$−SR−*HP1*. *HP2* was injected over the sensor surface at seven different concentrations (5.7, 11.3, 22.7, 45.3, 90.6, 181, 362.5, and 725 nM). (B) The $Z_{HER2:342}$−SR−*HP1*:*HP2* complex has a very slow dissociation rate, and 17 h after injection with 725 nM *HP2*, the dissociation is still <5% of the initial response. (C) Biacore sensorgrams of binding of prehybridized $Z_{HER2:342}$−SR−*HP1*:*HP2* to immobilized HER2 receptor. Six different concentrations (0.7, 1.5, 2.9, 5.9, 11.8, and 23.5 nM) of $Z_{HER2:342}$−SR−*HP1*:*HP2* were injected in duplicates over the HER2 sensor surface. All experiments in A−C were done in duplicate, and the sensorgrams are double-referenced by subtraction of a reference surface and a buffer injection. (D) Co-injection experiment showing the sequential binding of $Z_{HER2:342}$−SR−*HP1* and *HP2* to immobilized HER2. Step I shows the injection and binding of 1.2 μM $Z_{HER2:342}$−SR−*HP1* to HER2. This high concentration of $Z_{HER2:342}$−SR−*HP1* is expected to quickly saturate the HER2 surface with the Affibody−PNA chimera, and the response was normalized at 75 s after the start of the first injection. In the second injection step, 14.5 nM (green), 145 nM (red), and 1.45 μM (blue) *HP2* were allowed to hybridize to precaptured $Z_{HER2:342}$−SR−*HP1*. The gray line represents an injection of buffer control in the second injection step.

SR−*HP1*:*HP2* (Figure 4D). The dissociation of a PNA:PNA duplex is, in parallel to DNA duplex melting, associated with an increase in absorbance at 260 nm. This increase, which arises from the loss of base-stacking interactions, can be monitored using a UV−vis spectrophotometer with a temperature-controlled sample cell.[38] The *HP1*:*HP2* duplexes were determined to have very high melting temperatures, both on their own (86 °C) and in $Z_{HER2:342}$−SR−*HP1*:*HP2* (88 °C). UV melts of single-stranded *HP1*, *HP2*, and $Z_{HER2:342}$−SR−*HP1* (Figure 4E) all show an increase in absorbance at 260 nm over a broad temperature range. This behavior is suggested to be a consequence of the highly flexible PNA backbone, which allows for energetically favorable base-stacking interactions even in the absence of observable intra- or intermolecular hydrogen bonds.[56] Importantly, the absence of cooperative melting transitions in Figure 4E suggests that the single stranded probes do not self-hybridize.

Taken together, the spectroscopic characterization of *HP1* and *HP2* show that the probes can hybridize to form a structured *HP1*:*HP2* duplex with very high thermal stability (86 °C). Both the duplex secondary structure, investigated with CD spectroscopy, and the duplex stability, measured by UV thermal melts, are very similar in *HP1*:*HP2* and in $Z_{HER2:342}$−SR−*HP1*:*HP2*, suggesting that probe hybridization is largely unaffected by the attachment to the Affibody molecule. The thermal melting temperatures of $Z_{HER2:342}$−SR−H_6 and $Z_{HER2:342}$−SR−*HP1* as well as the previously published T_m for $Z_{HER2:342}$ all fall within 67 ± 1 °C, indicating that the Z scaffold is not destabilized by the post-translational conjugation to *HP1*.

Surface Plasmon Resonance Based Binding Analysis. Figure 5A shows representative surface plasmon resonance (SPR) sensorgrams of the hybridization of *HP2* to immobilized $Z_{HER2:342}$−SR−*HP1*. The rate constant for association, k_a, was estimated to be 1.7×10^5 M^{-1} s^{-1} for the interaction, but the dissociation rate constant, k_d, for *HP2* was found to be too slow to be measured by Biacore. An extended dissociation phase of up to 17 h (Figure 5B) resulted in a <5% reduction of the initial response and no k_d; thus, no equilibrium dissociation constant, K_D, could be determined for the interaction. The extremely slow dissociation rate shown here is in agreement with observations previously reported for complementary morpholinos and PNA-based oligonucleotides of similar lengths.[57,58] The interaction between prehybridized $Z_{HER2:342}$−SR−*HP1*:*HP2* and immobilized HER2 was studied to investigate if the Affibody−PNA chimera had retained affinity for the HER2 receptor (Figure 5C). The slowly dissociating $Z_{HER2:342}$−SR−*HP1*:*HP2* complex was expected to be stable during this (25 min) experiment. Our data show that the $Z_{HER2:342}$−SR−*HP1*:*HP2* complex experiences both a fast on-rate (1.4×10^6 M^{-1} s^{-1}) and a slow off-rate (2.9×10^{-4} s^{-1}). The χ^2 value, reflecting the fit to the kinetic model, was 0.586. The value of K_D was estimated to be 212 pM for the interaction, and this

DOI: 10.1021/acs.bioconjchem.5b00292
Bioconjugate Chem. 2015, 26, 1724−1736

Table 2. Biodistribution of ^{125}I-*HP2* and ^{111}In-*HP2* in NMRI Mice at 1 and 4 h p.i.[a]

	^{125}I-*HP2* 1 h	^{125}I-*HP2* 4 h	^{111}In-*HP2* 1 h	^{111}In-*HP2* 4 h
blood	0.63 ± 0.15[b]	0.21 ± 0.05	0.41 ± 0.06	0.15 ± 0.01[c]
lung	0.52 ± 0.11	0.24 ± 0.10[b]	0.56 ± 0.19	0.25 ± 0.15[c]
liver	0.19 ± 0.06[b]	0.09 ± 0.01[d]	0.83 ± 0.14[e]	0.82 ± 0.08
spleen	0.23 ± 0.06[b]	0.13 ± 0.02[d]	0.38 ± 0.20	0.48 ± 0.14
kidney	1.59 ± 0.30[b]	0.17 ± 0.04[d]	4.60 ± 1.19[e]	3.83 ± 0.39
stomach	2.02 ± 1.01	0.95 ± 0.25[d]	0.18 ± 0.06	0.12 ± 0.06
salivary gland	1.97 ± 0.57[b]	0.94 ± 0.39[d]	0.15 ± 0.01[e]	0.09 ± 0.01[c]
muscle	0.18 ± 0.04[b]	0.05 ± 0.01	0.12 ± 0.01	0.05 ± 0.00[c]
bone	0.14 ± 0.09	0.07 ± 0.02[d]	0.13 ± 0.09	0.15 ± 0.02
gastrointestinal tract[f]	0.73 ± 0.05	1.16 ± 0.40[d]	0.36 ± 0.07[e]	0.62 ± 0.38
carcass[f]	5.39 ± 1.31[b]	2.65 ± 0.77[d]	3.57 ± 0.32	1.79 ± 0.59

[a]Data are presented as an average % ID/g and standard deviation for 5 mice. [b]Difference was significant ($p < 0.05$) between normal organ uptake of ^{125}I-*HP2* at 1 and 4 h p.i. [c]Difference was significant ($p < 0.05$) between normal organ uptake of ^{111}In-*HP2* at 1 and 4 h p.i. [d]Difference was significant ($p < 0.05$) between normal organ uptake of ^{125}I-*HP2* and ^{111}In-*HP2* at 4 h p.i. [e]Difference was significant ($p < 0.05$) between normal organ uptake of ^{125}I-*HP2* and ^{111}In-*HP2* at 1 h p.i. [f]Data are presented as %ID per whole sample.

value is close to the dissociation equilibrium constants (90.2−283 pM) reported earlier for $Z_{HER2:342}$ variants carrying short C-terminal peptide extensions.[59] Compared to the 22 pM K_D of the $Z_{HER2:342}$ parental molecule, this is a slight increase, but as noted earlier by Wållberg et al., the K_D of $Z_{HER2:342}$ was determined using immobilized HER2−ECD and not HER2−ECD−Fc as in this current study.[4,59] In a co-injection experiment (Figure 5D), we investigated whether $Z_{HER2:342}$−SR−*HP1* could interact simultaneously with the HER2 receptor and *HP2*. A high concentration of $Z_{HER2:342}$−SR−*HP1*, which we expected to quickly saturate the HER2 surface with the Affibody−PNA chimera, was first injected and immediately followed by a secondary injection of *HP2*. The interaction between the captured $Z_{HER2:342}$−SR−*HP1* and *HP2* was confirmed by a saturable and concentration-dependent increase of the SPR signal upon injection of *HP2*, whereas an injection of buffer did not increase the response. To summarize, the SPR-based characterization indicates that interaction between $Z_{HER2:342}$−SR−*HP1* and *HP2* is very strong at room temperature. The interaction between the two complementary PNA-based probes is characterized by a moderately fast association rate constant combined with an extremely slow dissociation rate. A co-injection experiment showed that $Z_{HER2:342}$−SR−*HP1* was able to bind to immobilized HER2 and subsequently capture *HP2* in a concentration dependent manner. Prehybridized $Z_{HER2:342}$−SR−*HP1*:*HP2* show a retained picomolar binding affinity (212 pM) for the HER2 receptor, indicating that the conjugation to the *HP1*-probe and a subsequent hybridization to *HP2* does not sterically hinder the Affibody molecule binding to the receptor.

In Vivo Biodistribution Studies. A prerequisite for effective pretargeting using our proprosed PNA-based strategy is that the radiolabeled effector probe *HP2* has a favorable in vivo biodistribution profile with fast blood clearance and low accumulation of radioactivity in normal tissue including kidneys. An exploratory study was performed in normal NMRI mice to evaluate the general biodistribution profiles of both ^{125}I- and ^{111}In-labeled *HP2* (Table 2). Both ^{125}I- and ^{111}In-labeled *HP2* had very fast blood clearance: at 1 h post injection, the percentage of injected dose per gram of blood (%ID/g) was already down to 0.63 ± 0.15 and 0.41 ± 0.15 for ^{125}I- and ^{111}In-*HP2*, respectively. The low radioactivity in the gastrointestinal tract suggests that hepatobiliary excretion pathway played a minor role in the clearance. The kidneys show a low accumulation of both ^{125}I-*HP2* (1.59 ± 0.30%ID/g) and ^{111}In-*HP2* (4.60 ± 1.19%ID/g) at 1 h p.i., and the kidney uptake had reduced significantly ($p < 0.05$) at 4 h p.i. for both ^{125}I-*HP2* (0.17 ± 0.04%ID/g) and ^{111}In-*HP2* (3.83 ± 0.39% ID/g). As a comparison, the renal uptake of ^{111}In-labeled DOTA-conjugated $Z_{HER2:342}$ derivatives was (180−200%ID/g) at 4 h after injection in NMRI-mice, i.e., 45−50-fold higher.[60,61] The very fast blood clearance and the low kidney uptake of ^{111}In-*HP2* are in accordance with previously published biodistribution studies of ^{99m}Tc-labeled PNAs in normal mice and suggest that radiometal-labeled *HP2* is a promising effector probe candidate for pretargeted radionuclide therapy.[35]

Concluding Remarks. In this paper, we describe the design, solid-phase synthesis, and biophysical characterization of two complementary PNA-based hybridization probes, *HP1* and *HP2*, for use in pretargeted delivery of radionuclides in vivo. *HP1* is site-specifically and covalently attached using sortase A mediated ligation to a recombinantly expressed anti-HER2 Affibody molecule for specific delivery of the PNA-probe to HER2-expressing tumors. The produced Affibody−PNA chimera, $Z_{HER2:342}$−SR−*HP1*, is stable, well-structured, and capable of high-affinity binding in vitro to both the HER2 receptor and the complementary *HP2* probe. *HP2* is dually functionalized with a DOTA chelator and a tyrosine for radiolabeling with radiometals and radioiodine, respectively. Both ^{125}I- and ^{111}In-labeled *HP2* show favorable biodistribution profiles in normal mice with very fast blood clearance rates and low accumulation of radioactivity in kidneys and other tissues. Taken together, the data presented here suggest that a PNA-mediated strategy is a promising approach for pretargeting of Affibody molecules. In a follow-up proof-of-principle study, we show the feasibility of PNA-based Affibody-mediated pretargeting of HER2-expressing tumors in a mouse cancer model.[62] The PNA-based hybridization probes used here were synthesized in-house using commercial building blocks and standard equipment available in any peptide synthesis laboratory. Functionalities like different types of radiometal chelators for complexing of therapeutic radionuclides, or fluorescent probes for near-infrared in vivo imaging can easily be built into the probes making them highly customizable. We envision that the sortase A mediated ligation strategy presented here can be expanded to conjugate PNA-based hybridization probes not only to other Affibody molecules but also to other types of targeting agents such as full-length antibodies, antibody

DOI: 10.1021/acs.bioconjchem.5b00292
Bioconjugate Chem. 2015, 26, 1724−1736

fragments, and different types of antibody mimetics making PNA-mediated pretargeting more generally applicable.

EXPERIMENTAL PROCEDURES

Construction of Expression Plasmids. *Sortase A.* The plasmid pGBMCS-SortA, coding for a variant of *Staphylococcus aureus* sortase A in which the membrane anchoring domain, amino acids 1−59, has been deleted was provided by Addgene (Addgene plasmid no. 21931). In this construct, the enzyme is N-terminally fused to a protein G B1 domain to increase solubility and C-terminally to a hexahistidine tag to allow for protein purification using immobilized metal-ion-affinity chromatography (IMAC).[63] The gene construct is subcloned into a pET-21d(+) vector carrying genes coding for ampicillin resistance and IPTG-inducible protein expression via the T7 RNA polymerase/promoter system (Novagen).

$Z_{HER2:342}$−SR−H_6. The gene sequence of $Z_{HER2:342}$ was PCR amplified from pAY457-$Z_{HER2:342}$-ST, using primers that contained *Pst*I and *Acc*I restriction sites and subcloned into a pAY430 vector.[4,64] pAY457-$Z_{HER2:342}$-ST and pAY430 were kind gifts from Helena Wållberg (Karolinska Institutet, Sweden). pAY457 and pAY430 are both pET-derived vectors, carrying genes coding for kanamycin resistance, and the protein expression is under control of a T7 promotor.[64]

An N-terminal His_6 tag and subsequent TEV protease recognition site were removed together by introduction of a second *Nde*I restriction site (underlined) on the 5′ end of the $Z_{HER2:342}$ gene via PCR amplification with the primers 5′-TTTATTTTCATATGGTAGATAACAAATTCACAAAGA-AATGCGAAAC-3′ and 5′-GATTTTCCTGCAGGTGATG-3′. The plasmid was double digested with *Nde*I, purified using agarose-gel electrophoresis, and the larger DNA fragment religated using T4 DNA ligase (New England Biolab) producing pAY430-$Z_{HER2:342}$-VD.

A DNA segment coding for (i) a $(GS)_3$-linker (marked in italics in the sequence below), (ii) an optimized sortase A recognition motif, LPETGG, (marked in bold), and (iii) a hexahistidine tag (in square brackets) followed by two TAA stop codons and flanked by *Acc*I and *Bam*HI restriction sites (underlined) at the 5′ and 3′ ends, respectively, was ordered from Eurofins Genomics.[47] Nine scrambled nucleotides flank the restriction sites on each side. 5′-TAATAAGCAGTAGAC-*GGCAGCGGCAGCGGCAGC***CTGCCGGAAACCGGCGGC**-[CATCACCATCACCATCAC]TAATAAAAGCTT-GACGACAAT-3′

pAY430-$Z_{HER2:342}$-SR-H_6 was produced by PCR amplification of the DNA segment. The PCR product was then cut with *Acc*I and *Bam*HI (New England Biolab) and ligated into the likewise-cut pAY430-$Z_{HER2:342}$-VD. All DNA sequences were verified using sequencing (Eurofins Genomics).

The resulting 78-residue amino acid sequence of $Z_{HER2:342}$−SR−H_6 is shown below. Surrounded by bullets is the original $Z_{HER2:342}$ sequence, residues 1−58, and the C-terminal −SR−H_6 extension, residues 59−78, is marked in accordance with the DNA sequence above. •VDNKFNKEMRNAYWEIAL-LPNLNNQQKRAFIRSLYDDPSQSANLLAEAKKLNDA-QAPK•VD*GSGSGS***LPETGG**[HHHHHH]

Expression and Purification of Recombinant Proteins. *General Protein Expression and Purification.* Plasmids pGBMCS-SortA and pAY430-$Z_{HER2:342}$-SR were transformed into chemically competent BL21-Star (DE3) *E. coli* cells (Life Technologies). Cells were cultivated in trypticase soy yeast extract broth, and following protein induction with 1 mM IPTG, cultures were left to incubate at 25 °C with shaking (180 rpm) for 19−22 h and harvested by centrifugation. Cell pellets were resuspended in IMAC binding buffer (25 mM NaH_2PO_4, 150 mM NaCl, 10 mM imidazole, pH 7) and lysed by sonication. The lysate was clarified using centrifugation, passed over a Talon Metal Affinity Resin (Takara Bio Inc., Japan) and eluted with IMAC elution buffer (25 mM NaH_2PO_4, 150 mM NaCl, 300 mM imidazole, pH 7).

Sortase A was concentrated to 1 mM in sortase A storage buffer (50 mM Tris base, 150 mM NaCl, 10% glycerol, pH 7.5) using an Amicon ultra concentrator with a 10 K molecular weight cut off (Amicon Ultra-15, Merck Milipore, Ireland) and was stored in 50 μL aliquots at −80 °C.

$Z_{HER2:342}$−SR−H_6 was lyophilized following IMAC purification, and salts and imidazole were removed by gel filtration (PD-10, GE Healthcare). The Affibody molecule was then stored at a concentration of 0.5 mM in sortase A ligation buffer (50 mM Tris base, 150 mM NaCl, 10 mM $CaCl_2$, pH 7.5) at −20 °C.

Extinction coefficients at 280 nm (Σ_{280}) for sortase A and $Z_{HER2:342}$−SR−H_6, 24 410 and 8 480 M^{-1} cm^{-1}, respectively, were estimated on the basis of their amino acid sequences using the ProtParam software (Swiss Institute of Bioinformatics).

Synthesis and Purification of Pretargeting Hybridization Probes. *General Synthesis.* The hybridization probes, *HP1* and *HP2*, were prepared by manual solid-phase synthesis using commercially available building blocks. All standard 9-fluorenylmethoxycarbonyl (Fmoc)-protected amino acids were provided by Novabiochem or Iris Biotech. Fmoc/benzhydryloxycarbonyl (Bhoc)-protected PNA monomers and the spacer molecule AEEA (Fmoc-8-amino-3,6-dioxaoctanoic acid) were all purchased from Polyorg, Inc. (USA). The macrocyclic chelator 1,4,7,10-tetraazacyclododecane-1,4,7,10-tetraacetic acid (DOTA) was incorporated into synthesis as a DOTA-tri(tBu)-ester and was obtained from Macrocyclics (USA). Acylation reactions were performed with five molar excess of monomer (amino acid, PNA, AEEA, or DOTA) in *N*-methyl-2-pyrrolidone (NMP) activated with 5 equiv of activator and base. The activator was a solution of benzotriazol-1-yl-oxytripyrrolidinophosphonium hexafluorophosphate (PyBOP; Sigma-Aldrich) in dimethylformamide (DMF) and was freshly prepared before each acylation reaction. The base for PNA:amino acid or PNA:PNA couplings was a solution of 0.2 M N,N-diisopropylethylamine (DIEA) and 0.2 M 2,6-lutidine (Sigma-Aldrich) in NMP. For all other coupling reactions, 0.4 M DIEA in NMP was used as base. All acylation reactions were performed at room temperature with gentle shaking, and coupling times for all monomers ranged from 45 min to 2 h. Kaiser tests were performed to monitor the completion of each acylation reaction, and the coupling procedure was repeated a second time with fresh reagents when needed. Unreacted amino groups were capped with acetic acid/2,6-lutidine/NMP (5:6:89) for 10 min. Deprotection of the Fmoc group was carried out in 20% piperidine in NMP for 20 min. *HP1* and *HP2* were deprotected and cleaved off the resin upon completion of synthesis by treatment with trifluoracetic acid (TFA)/triisopropylsilane (TIS)/H_2O (95:2.5:2.5) for 3 h at room temperature. The hybridization probes were then extracted three times using 50% *tert*-butyl methyl ether in water and lyophilized.

Synthesis of HP1. Synthesis of *HP1* (Scheme 1) was performed in a 50 μmol scale on an acid-labile Rink-amide ChemMatrix resin with a substitution level of 0.6 mmol g^{-1}

DOI: 10.1021/acs.bioconjchem.5b00292
Bioconjugate Chem. 2015, 26, 1724−1736

(Sigma-Aldrich). First, the C-terminal part of the molecule, (E−K(DOTA)−AEEA−E), was assembled. The negatively charged amino acid Glu was coupled to the solid support, using Fmoc−Glu(OtBu)−OH, followed by the hydrophilic, PEG-based linker molecule AEEA and a 4-methyltrityl (Mtt)-protected Lys (Fmoc−Lys(Mtt)−OH; Iris Biotech). The acid-labile Mtt group was then specifically cleaved off by treatment with 1% TFA in dichloromethane (DCM) for 10 × 2 min, and the chelator DOTA was coupled to the free amine on the lysine side chain. Next, another Glu was incorporated, finishing the C-terminal part of the molecule. The PNA hybridization part (agt ctg gat gta gtc) was added next and was assembled using Fmoc−PNA−A(Bhoc)−OH, Fmoc−PNA−C(Bhoc)−OH, Fmoc−PNA−C(Bhoc)−OH, and Fmoc−PNA−T−OH. Lastly, the probe was extended with the N-terminal part (G−G−G−S−S) by coupling two polar Ser residues and three Gly, using Fmoc−Ser(tBu)−OH and Fmoc−Gly−OH respectively, to the growing molecule.

Synthesis of HP2. The synthesis of *HP2* was done in the same scale and using the same reagents as the synthesis of *HP1* described above. Fmoc−Tyr(tBu)−OH was used to couple Tyr to the resin, to allow for probe iodine labeling, and next, two Glu residues were coupled in succession. The PNA part of the molecule (gac tac atc cag act), complementary to the PNA sequence in *HP1*, was then added sequentially, followed by two Ser residues and an AEEA monomer. Coupling of the chelator DOTA to the deprotected amino group in AEEA concluded the synthesis of *HP2*.

Analysis and Purification. Synthesis crudes were resuspended in 0.1% TFA in water and filtered through a 0.45 μm PVDF membrane before being subjected to purification using HPLC. All HPLC purification steps were performed on a semipreparative Zorbax C_{18} column (300SB-C18, 9.4 × 250 mm^2, 5 μm pore size; Agilent) with an elution gradient going from 0 to 30% B (A: 0.1% TFA/H_2O; B: 0.1% TFA/CH_3CN) in 30 min and a flow rate of 3 mL/min. An elevated column temperature of 45 °C was used to improve separation. Purity analysis of *HP2* was performed under the same conditions as the HPLC purification step, and the correct molecular weights of *HP1* and *HP2* were verified using ESI-Q-TOF-MS. Hybridization probe molar extinction coefficients at 260 nm, Σ_{260}, used throughout this article are 155 800 and 150 700 $M^{-1}cm^{-1}$ for *HP1* and *HP2*, respectively. The extinction coefficients were estimated as the sum of the monomeric extinction coefficients for their respective PNA sequence (A: 13 700 $M^{-1}cm^{-1}$, C: 6 600 $M^{-1}cm^{-1}$, G: 11 700 $M^{-1}cm^{-1}$, and T: 8 600 $M^{-1}cm^{-1}$). PNA monomeric extinction coefficients were obtained from Applied Biosystems.

Sortase A Mediated $Z_{HER2:342}$−SR−HP1 Ligation. *HP1* (30 nmol) was dissolved together with $Z_{HER2:342}$−SR−H_6 (120 nmole) in 500 μL of ligation buffer, and the pH of the solution was adjusted to 7.5 using 50% NaOH. The ligation reaction was started by the addition of 5 μM sortase A and left to proceed for 15−24 h at room temperature on a rotating tube shaker. To quench the reaction, 500 μL of Talon metal affinity resin, pre-equilibrated in IMAC binding buffer, was added to the ligation mixture. Following a 30 min incubation, the mixture was added to an empty flow column, and the flow-through, containing the ligation product $Z_{HER2:342}$−SR−*HP1*, unreacted *HP1*, and hydrolyzed byproducts missing the hexahistidine tag, was collected, lyophilized, and subjected to PD-10 gel filtration. A final HPLC separation step was performed under the same conditions as previously described for purification of the hybridization probes but with a modified elution gradient (10−45% B in 35 min). The ligation efficiency (on the basis of *HP1*) was evaluated by comparing integrated areas under the peaks in the HPLC chromatogram at 260 nm. The purity of $Z_{HER2:342}$−SR−*HP1* and *HP2* was analyzed with HPLC, using the same column as for the purification but with modified elution gradients (20−40% B in 20 min for $Z_{HER2:342}$−SR−*HP1* and 0−25% B in 25 min for *HP2*) and determined by comparing integrated areas under the peaks in the HPLC elution profile at 220 nm. Unreacted *HP1* was pooled separately and reused in new ligation reactions together with fresh $Z_{HER2:342}$−SR−H_6.

Characterization of Proteins, Hybridization Probes, and Chimeras. A Σ_{260} of 155 800 M^{-1} cm^{-1} was used for concentration determination of the $Z_{HER2:342}$−SR−*HP1* Affibody probe chimera throughout this article because the absorbance of the PNA-based probe was estimated to dominate the total absorbance at 260 nm. A protein absorbs much less light than a nucleic acid at 260 nm, and in a 1:1 nucleic acid/protein mixture, the protein contributes with about 2% to the total absorbance at 260 nm.[65]

All CD studies were performed on a Jasco J-810 CD spectrometer equipped with a Peltier thermoelectric controller. Proteins, hybridization probes and chimeras were dissolved in 20 mM potassium phosphate buffer with 100 mM KCl (pH 7.4). All CD measurements were performed in a capped fluorescence cell with a 0.1 cm path length. Unfolding of $Z_{HER2:342}$−SR−H_6 and $Z_{HER2:342}$−SR−*HP1* in the absence or presence of *HP2* was monitored by measuring the ellipticity at 221 nm, θ_{221}, as a function of temperature. Temperature was increased between 20 and 90 °C in 0.1 °C increments at a speed of 5 °C/min. After denaturation, the temperature in the cuvette was returned to 20 °C to monitor signal recovery at 221 nm.

UV melts were performed on a Varian Cary 50 Bio UV−visual spectrophotometer equipped with a single-cell Peltier thermostatted cuvette holder. All samples, both single-stranded molecules and prehybridized duplexes, were diluted to a concentration of 5 μM in 20 mM potassium phosphate buffer with 100 mM KCl (pH 7.4) and transferred to a capped quartz cell with a 1.0 cm path length. The temperature in the cell was adjusted at a speed of 0.5 °C/min between 20−70 °C for the single-stranded molecules and 20−95 °C for prehybridized duplexes, and measurements were taken at 260 nm after a 60 s equilibration at each temperature point.

All T_m values were defined as the maximum of the first derivative of their respective melting curves.

Surface Plasmon Resonance Based Binding analysis. *General Surface Plasmon Resonance.* All SPR measurements were conducted on a Biacore 3000 system (GE Healthcare) with carboxymethylated dextran coated gold sensor chips (CM5) at 25 °C. The running buffer, which was also used for analyte dilution, was degassed PBS-T (10 mM Na_2HPO_4, 150 mM NaCl and 0.005% Tween-20; pH 7.4), and the flow rate was 50 μL/min in all experiments. Standard NHS/EDC coupling was used to immobilize the ligand covalently to the chip, and following immobilization, the surface was capped with ethanolamine. A reference surface was prepared on each chip by activating the chip surface and then immediately capping it without any ligand immobilization.

For analysis of *HP2* binding to $Z_{HER2:342}$−SR−*HP1*, 170 RU (resonance units) of $Z_{HER2:342}$−SR−*HP1* was immobilized on the surface of a sensor chip. *HP2* was injected over the chip surface at seven different concentrations ranging from 5.7 to

DOI: 10.1021/acs.bioconjchem.5b00292
Bioconjugate Chem. 2015, 26, 1724−1736

725 nM, and binding was analyzed with a 5 min association phase followed by a 20 min dissociation phase. The ligand surface was regenerated to dissociate the bound analyte from the covalently immobilized ligand with a 30 s injection of 15 mM HCl immediately followed by a 30 s injection of 25% ethylene glycol in water. The chip was then left to stabilize in running buffer for 20 min before the next sample injection. To further study the dissociation phase of the binding process, the dissociation time was increased to 17 h for the sample with the highest concentration of *HP2* (725 nM).

Binding of $Z_{HER2:342}$−SR−*HP1*:*HP2* ($Z_{HER2:342}$−SR−*HP1* hybridized to the complementary *HP2* probe) to the extracellular part of the HER2 receptor was analyzed using Biacore. Equal volumes of $Z_{HER2:342}$−SR−*HP1* (3.4 μM) and *HP2* (3.7 μM) were heated to 65 °C, mixed, and left to hybridize for at least 15 min on ice to form $Z_{HER2:342}$−SR−*HP1*:*HP2*. Following hybridization, $Z_{HER2:342}$−SR−*HP1*:*HP2* was diluted in SPR running buffer and used for binding analysis without further purification. Approximately 600 RU of recombinant human HER2/Fc chimera (Sino Biologicals) was immobilized on a CM5 chip and kinetic information was then obtained by flowing a dilution series in duplicate of hybridized $Z_{HER2:342}$−SR−*HP1*:*HP2* (0.7, 1.5, 2.9, 5.9, 11.8, and 23.5 nM) over the immobilized receptor. Association and dissociation times were 300 and 1200 s, respectively, and the surface was regenerated with a short pulse of 10 mM HCl following each experiment. The results were fitted to a 1:1 Langmuir binding model for calculation of the kinetic parameters.

A co-injection study of the sequential binding of $Z_{HER2:342}$−SR−*HP1* and *HP2* to immobilized HER2 receptor was performed using the co-inject command in the Biacore control software. The same HER2 chip as in the $Z_{HER2:342}$−SR−*HP1*:*HP2* binding experiment was used for the co-injection study. A 100 μL aliquot of 1.2 μM $Z_{HER2:342}$−SR−*HP1* was injected over the HER2 chip surface and expected to quickly saturate the surface with the Affibody−PNA chimera. In the second step, 250 μL of 14.5, 145, or 1450 nM *HP2* or a buffer control was injected over the precaptured $Z_{HER2:342}$−SR−*HP1*. The ligand surface was regenerated with HCl and ethylene glycol as previously described for the analysis of *HP2* binding to $Z_{HER2:342}$−SR−*HP1*.

In Vivo Evaluation of Radiolabeled *HP2*. The animal experiment was performed in accordance with national legislation on laboratory animal protection and had been approved by the ethics committee for Animal Research in Uppsala. Euthanasia was performed under Rompun/Ketalar anesthesia.

For labeling of *HP2* with ^{111}In, the lyophilized conjugate (50 μg) was reconstituted in 50 μL of 0.2 M ammonium acetate, pH 5.5, mixed with 15 MBq ^{111}In stock solution and incubated at 90 °C for 15 min. After labeling, the radio-conjugate was purified using a NAP-5 size-exclusion column equilibrated with PBS.

For radioiodination of *HP2*, 50 μg of *HP2*, 1.1 μg/μL in PBS, was mixed with 12 MBq ^{125}I in 30 μL. The reaction was initiated by adding 5 μg chloramine-T (1 mg/mL in PBS), and the mixture was incubated for 2 min at room temperature. The reaction was ceased by addition of 10 μL of sodium metabisulfite (5 mg/mL PBS) and purified using NAP-5 columns (GE Healthcare).

Measurements of labeling yield and radiochemical purity of conjugates were performed by radio-instant thin-layer chromatography (ITLC) cross-validated by radio-SDS-PAGE (200 V constant). ITLC was eluted using 0.2 M citric acid, pH 2.0, for ^{111}In or with acetone/water (8:2). In both cases, conjugates remained at application points, and free radionuclide migrated with the solvent front. The labeling yields of ^{111}In-*HP2* and ^{125}I-*HP2* were 97 and 85%, respectively. The purity of conjugates after NAP-5 purification was 99.3 and 99.9% for ^{111}In-*HP2* and ^{125}I-*HP2*, respectively.

Female NMRI mice (average weight = 27 ± 1 g) were co-injected with 20 kBq (1 μg) of ^{111}In-*HP2* and 10 kBq (1 μg) of ^{125}I-*HP2* in 100 μL of PBS, and biodistribution was measured at 1 and 4 h p.i. A group of 4 mice was used for each data point. The mice were euthanized by overdosing of anesthesia followed by heart puncture and exsanguination. Blood and organ samples were collected, and their weight and radioactivity were measured. Whole spectra of each sample were recorded. For ^{125}I measurements, counts in the energy window of 6−80 keV were integrated; for ^{111}In, counts from the window of 100−500 keV were integrated. The data were corrected for background, dead time, and spillover. Organ uptake values were calculated as percent of injected dose per gram of tissue (%ID/g).

AUTHOR INFORMATION

Corresponding Author

*School of Biotechnology, Division of Protein Technology, KTH Royal Institute of Technology, AlbaNova University Center, 106 91 Stockholm, Sweden. Phone: +46 8 5537 8333. Fax: +46 8 5537 8481. E-mail: amelie@biotech.kth.se.

Notes

The authors declare no competing financial interest.

ACKNOWLEDGMENTS

This research was financially supported by grants from the Swedish Cancer Society (grant 2012/354) and the Swedish Research Council (grants 521-2012-2228 and 621-2013-5135).

REFERENCES

(1) Barbet, J., Bardiès, M., Bourgeois, M., Chatal, J. F., Chérel, M., Davodeau, F., Faivre-Chauvet, A., Gestin, J. F., and Kraeber-Bodéré, F. (2012) Radiolabeled antibodies for cancer imaging and therapy. *Methods Mol. Biol. 907*, 681−697.

(2) Kraeber-Bodéré, F., Bodet-Milin, C., Rousseau, C., Eugène, T., Pallardy, A., Frampas, E., Carlier, T., Ferrer, L., Gaschet, J., Davodeau, F., et al. (2014) Radioimmunoconjugates for the treatment of cancer. *Semin. Oncol. 41*, 613−622.

(3) Wikman, M., Steffen, A. C., Gunneriusson, E., Tolmachev, V., Adams, G. P., Carlsson, J., and Ståhl, S. (2004) Selection and characterization of HER2/neu-binding affibody ligands. *Protein Eng., Des. Sel. 17*, 455−462.

(4) Orlova, A., Magnusson, M., Eriksson, T. L., Nilsson, M., Larsson, B., Höidén-Guthenberg, I., Widström, C., Carlsson, J., Tolmachev, V., Ståhl, S., and Nilsson, F. Y. (2006) Tumor imaging using a picomolar affinity HER2 binding affibody molecule. *Cancer Res. 66*, 4339−4348.

(5) Friedman, M., Orlova, A., Johansson, E., Eriksson, T. L., Höidén-Guthenberg, I., Tolmachev, V., Nilsson, F. Y., and Ståhl, S. (2008) Directed evolution to low nanomolar affinity of a tumor-targeting epidermal growth factor receptor-binding affibody molecule. *J. Mol. Biol. 376*, 1388−1402.

(6) Kronqvist, N., Malm, M., Göstring, L., Gunneriusson, E., Nilsson, M., Höidén-Guthenberg, I., Gedda, L., Frejd, F. Y., Ståhl, S., and Löfblom, J. (2011) Combining phage and staphylococcal surface display for generation of ErbB3-specific Affibody molecules. *Protein Eng., Des. Sel. 24*, 385−396.

DOI: 10.1021/acs.bioconjchem.5b00292
Bioconjugate Chem. 2015, 26, 1724−1736

(7) Li, J., Lundberg, E., Vernet, E., Larsson, B., Höidén-Guthenberg, I., and Gräslund, T. (2010) Selection of affibody molecules to the ligand-binding site of the insulin-like growth factor-1 receptor. *Biotechnol. Appl. Biochem. 55*, 99−109.
(8) Honarvar, H., Garousi, J., Gunneriusson, E., Höidén-Guthenberg, I., Altai, M., Widström, C., Tolmachev, V., and Frejd, F. Y. (2014) Imaging of CAIX-expressing xenografts in vivo using 99mTc-HEHEHE-ZCAIX:1 affibody molecule. *Int. J. Oncol. 46*, 513−520.
(9) Feldwisch, J., and Tolmachev, V. (2012) Engineering of affibody molecules for therapy and diagnostics. *Methods Mol. Biol. 899*, 103−126.
(10) Frampas, E., Rousseau, C., Bodet-Milin, C., Barbet, J., Chatal, J. F., and Kraeber-Bodéré, F. (2013) Improvement of radioimmunotherapy using pretargeting. *Front. Oncol. 3*, No. 00159, DOI: 10.3389/fonc.2013.00159.
(11) Knight, J. C., and Cornelissen, B. (2014) Bioorthogonal chemistry: implications for pretargeted nuclear (PET/SPECT) imaging and therapy. *Am. J. Nucl. Med. Mol. Imaging 4*, 96−113.
(12) van de Watering, F. C., Rijpkema, M., Robillard, M., Oyen, W. J., and Boerman, O. C. (2014) Pretargeted imaging and radioimmunotherapy of cancer using antibodies and bioorthogonal chemistry. *Front. Med. 1*, No. 00044, DOI: 10.3389/fmed.2014.00044.
(13) Hnatowich, D. J., Virzi, F., and Rusckowski, M. (1987) Investigations of avidin and biotin for imaging applications. *J. Nucl. Med. 28*, 1294−1302.
(14) Liu, G., and Hnatowich, D. J. (2008) A semiempirical model of tumor pretargeting. *Bioconjugate Chem. 19*, 2095−2104.
(15) Knox, S. J., Goris, M. L., Tempero, M., Weiden, P. L., Gentner, L., Breitz, H., Adams, G. P., Axworthy, D., Gaffigan, S., Bryan, K., et al. (2000) Phase II trial of yttrium-90-DOTA-biotin pretargeted by NR-LU-10 antibody/streptavidin in patients with metastatic colon cancer. *Clin. Cancer Res. 6*, 406−414.
(16) Rusckowski, M., Fogarasi, M., Virzi, F., and Hnatowich, D. J. (1995) Influence of endogenous biotin on the biodistribution of labelled biotin derivatives in mice. *Nucl. Med. Commun. 16*, 38−46.
(17) Rosebrough, S. F. (1993) Plasma stability and pharmacokinetics of radiolabeled deferoxamine-biotin derivatives. *J. Pharmacol. Exp. Ther. 265*, 408−415.
(18) Reardan, D. T., Meares, C. F., Goodwin, D. A., McTigue, M., David, G. S., Stone, M. R., Leung, J. P., Bartholomew, R. M., and Frincke, J. M. (1985) Antibodies against metal chelates. *Nature 316*, 265−268.
(19) Gautherot, E., Bouhou, J., Le Doussal, J. M., Manetti, C., Martin, M., Rouvier, E., and Barbet, J. (1997) Therapy for colon carcinoma xenografts with bispecific antibody-targeted, iodine-131-labeled bivalent hapten. *Cancer 80*, 2618−2623.
(20) Rossin, R., Renart Verkerk, P., van den Bosch, S. M., Vulders, R. C., Verel, I., Lub, J., and Robillard, M. S. (2010) In vivo chemistry for pretargeted tumor imaging in live mice. *Angew. Chem., Int. Ed. 49*, 3375−3378.
(21) Devaraj, N. K., Thurber, G. M., Keliher, E. J., Marinelli, B., and Weissleder, R. (2012) Reactive polymer enables efficient in vivo bioorthogonal chemistry. *Proc. Natl. Acad. Sci. U.S.A. 109*, 4762−4767.
(22) Zeglis, B. M., Sevak, K. K., Reiner, T., Mohindra, P., Carlin, S. D., Zanzonico, P., Weissleder, R., and Lewis, J. S. (2013) A pretargeted PET imaging strategy based on bioorthogonal Diels-Alder click chemistry. *J. Nucl. Med. 54*, 1389−1396.
(23) Rossin, R., van den Bosch, S. M., Ten Hoeve, W., Carvelli, M., Versteegen, R. M., Lub, J., and Robillard, M. S. (2013) Highly reactive trans-cyclooctene tags with improved stability for Diels-Alder chemistry in living systems. *Bioconjugate Chem. 24*, 1210−1217.
(24) Rossin, R., van Duijnhoven, S. M., Läppchen, T., van den Bosch, S. M., and Robillard, M. S. (2014) Trans-cyclooctene tag with improved properties for tumor pretargeting with the diels-alder reaction. *Mol. Pharmaceutics 11*, 3090−3096.
(25) Liu, G., Mang'era, K., Liu, N., Gupta, S., Rusckowski, M., and Hnatowich, D. J. (2002) Tumor pretargeting in mice using (99m)Tc-labeled morpholino, a DNA analog. *J. Nucl. Med. 43*, 384−391.
(26) Liu, G., Dou, S., Baker, S., Akalin, A., Cheng, D., Chen, L., Rusckowski, M., and Hnatowich, D. J. (2010) A preclinical 188Re tumor therapeutic investigation using MORF/cMORF pretargeting and an antiTAG-72 antibody CC49. *Cancer Biol. Ther. 10*, 767−774.
(27) Liu, G., Dou, S., Liu, Y., Wang, Y., Rusckowski, M., and Hnatowich, D. J. (2011) 90Y labeled phosphorodiamidate morpholino oligomer for pretargeting radiotherapy. *Bioconjugate Chem. 22*, 2539−2545.
(28) Nielsen, P. E., Egholm, M., and Buchardt, O. (1994) Peptide nucleic acid (PNA). A DNA mimic with a peptide backbone. *Bioconjugate Chem. 5*, 3−7.
(29) Nielsen, P. E. (1999) Peptide nucleic acid. A molecule with two identities. *Acc. Chem. Res. 32*, 624−630.
(30) Egholm, M., Buchardt, O., Christensen, L., Behrens, C., Freier, S. M., Driver, D. A., Berg, R. H., Kim, S. K., Norden, B., and Nielsen, P. E. (1993) PNA hybridizes to complementary oligonucleotides obeying the Watson-Crick hydrogen-bonding rules. *Nature 365*, 566−568.
(31) Demidov, V. V., Potaman, V. N., Frank-Kamenetskii, M. D., Egholm, M., Buchard, O., Sönnichsen, S. H., and Nielsen, P. E. (1994) Stability of peptide nucleic acids in human serum and cellular extracts. *Biochem. Pharmacol. 48*, 1310−1313.
(32) Cutrona, G., Boffa, L. C., Mariani, M. R., Matis, S., Damonte, G., Millo, E., Roncella, S., and Ferrarini, M. (2007) The peptide nucleic acid targeted to a regulatory sequence of the translocated c-myc oncogene in Burkitt's lymphoma lacks immunogenicity: follow-up characterization of PNAEμ-NLS. *Oligonucleotides 17*, 146−150.
(33) Upadhyay, A., Ponzio, N. M., and Pandey, V. N. (2008) Immunological Response to Peptide Nucleic Acid and its Peptide Conjugate Targeted to Transactivation Response (TAR) Region of HIV-1 RNA Genome. *Oligonucleotides 18*, 329−335.
(34) Ray, A., and Nordén, B. (2000) Peptide nucleic acid (PNA): its medical and biotechnical applications and promise for the future. *FASEB J. 14*, 1041−1060.
(35) Mardirossian, G., Lei, K., Rusckowski, M., Chang, F., Qu, T., Egholm, M., and Hnatowich, D. J. (1997) In vivo hybridization of technetium-99m-labeled peptide nucleic acid (PNA). *J. Nucl. Med. 28*, 907−913.
(36) McMahon, B. M., Mays, D., Lipsky, J., Stewart, J. A., Fauq, A., and Richelson, E. (2002) Pharmacokinetics and tissue distribution of a peptide nucleic acid after intravenous administration. *Antisense Nucleic Acid Drug Dev. 12*, 65−70.
(37) Rusckowski, M., Qu, T., Chang, F., and Hnatowich, D. J. (1997) Pretargeting using peptide nucleic acid. *Cancer 80*, 2699−2705.
(38) Totsingan, F., Jain, V., Bracken, W. C., Faccini, A., Tedeschi, T., Marchelli, R., Corradini, R., Kallenbach, N. R., and Green, M. M. (2010) Conformational Heterogeneity in PNA:PNA Duplexes. *Macromolecules 43*, 2692−2703.
(39) Armitage, B., Ly, D., Koch, T., Frydenlund, H., Ørum, H., and Schuster, G. B. (1998) Hairpin-forming peptide nucleic acid oligomers. *Biochemistry 37*, 9417−9425.
(40) Armitage, B. A. (2003) The impact of nucleic acid secondary structure on PNA hybridization. *Drug Discovery Today 8*, 222−228.
(41) Hunter, W. M., and Greenwood, F. C. (1962) Preparation of iodine-131 labelled human growth hormones of high specific activity. *Nature 194*, 495−496.
(42) Wilbur, D. S. (1992) Radiohalogenation of proteins: an overview of radionuclides, labeling methods, and reagents for conjugate labeling. *Bioconjugate Chem. 3*, 433−470.
(43) Nielsen, P. E., and Egholm, M. (1999) An Introduction to Peptide Nucleic Acid. *Curr. Issues Mol. Biol. 1*, 89−104.
(44) Nielsen, P. E., Haaima, G., Lohse, A., and Buchardt, O. (1996) Peptide Nucleic Acids (PNA) containing thymine monomers derived from chiral amino acids: Hybridization and solubility properties of D-lysine PNA. *Angew. Chem., Int. Ed. Engl. 35*, 1939−1942.
(45) Wållberg, H., Orlova, A., Altai, M., Hosseinimehr, S. J., Widström, C., Malmberg, J., Ståhl, S., and Tolmachev, V. (2011) Molecular design and optimization of 99mTc-labeled recombinant affibody molecules improves their biodistribution and imaging properties. *J. Nucl. Med. 52*, 461−469.

DOI: 10.1021/acs.bioconjchem.5b00292
Bioconjugate Chem. 2015, 26, 1724−1736

(46) de Koning, M. C., van der Marel, G. A., and Overhand, M. (2003) Synthetic developments towards PNA-peptide conjugates. *Curr. Opin. Chem. Biol. 7*, 734−740.
(47) McCluskey, A. J., and Collier, R. J. (2013) Receptor-directed chimeric toxins created by sortase-mediated protein fusion. *Mol. Cancer Ther. 12*, 2273−2281.
(48) Leung, M. K., Hagemeyer, C. E., Johnston, A. P., Gonzales, C., Kamphuis, M. M., Ardipradja, K., Such, G. K., Peter, K., and Caruso, F. (2012) Bio-click chemistry: enzymatic functionalization of PEGylated capsules for targeting applications. *Angew. Chem., Int. Ed. 51*, 7132−7136.
(49) Löfblom, J., Feldwisch, J., Tolmachev, V., Carlsson, J., Ståhl, S., and Frejd, F. Y. (2010) Affibody molecules: engineered proteins for therapeutic, diagnostic and biotechnological applications. *FEBS Lett. 584*, 2670−2680.
(50) Mazmanian, S. K., Liu, G., Ton-That, H., and Schneewind, O. (1999) Staphylococcus aureus sortase, an enzyme that anchors surface proteins to the cell wall. *Science 285*, 760−763.
(51) Popp, M. W., and Ploegh, H. L. (2011) Making and breaking peptide bonds: protein engineering using sortase. *Angew. Chem., Int. Ed. 50*, 5024−5032.
(52) Ritzefeld, M. (2014) Sortagging: a robust and efficient chemoenzymatic ligation strategy. *Chem. - Eur. J. 20*, 8516−8529.
(53) Warden-Rothman, R., Caturegli, I., Popik, W., and Tsourkas, A. (2013) Sortase-tag expressed protein ligation: Combing protein purification and site-specific bioconjugation into a single step. *Anal. Chem. 85*, 11090−11097.
(54) Pritz, S., Wolf, Y., Kraetke, O., Klose, J., Bienert, M., and Beyermann, M. (2007) Synthesis of biologically active peptide nucleic acid-peptide conjugates by sortase-mediated ligation. *J. Org. Chem. 72*, 3909−3912.
(55) Corradini, R., Tedeschi, T., Sforza, S., and Marchelli, R. (2012) Electronic circular dichroism of peptide nucleic acids and their analogues. In *Comprehensive Chiroptical Spectroscopy: Applications in Stereochemical Analysis of Synthetic Compounds, Natural Products, and Biomolecules* (Berova, N., Polavarapu, P. L., Nakanishi, K., and Woody, R. W., Eds.), Vol. 2, Chapter 18, John Wiley & Sons, Inc., Hoboken, NJ.
(56) Chen, S., Mohan, V., Kiely, J. S., Griffith, M. C., and Griffey, R. H. (1994) Molecular dynamics and NMR studies of single-stranded PNAs. *Tetrahedron Lett. 35*, 5105−5108.
(57) He, J., Liu, G., Zhang, S., Vanderheyden, J. L., Liu, N., Liu, C., Zhang, Y., Gupta, S., Rusckowski, M., and Hnatowich, D. J. (2003) A comparison of in vitro and in vivo stability in mice of two morpholino duplexes differing in chain length. *Bioconjugate Chem. 14*, 1018−1023.
(58) Wang, Y., Chang, F., Zhang, Y., Liu, N., Liu, G., Gupta, S., Rusckowski, M., and Hnatowich, D. J. (2001) Pretargeting with amplification using polymeric peptide nucleic acid. *Bioconjugate Chem. 12*, 807−816.
(59) Wållberg, H., Löfdahl, P.-A., Tschapalda, K., Uhlén, M., Tolmachev, V., Nygren, P.-A., and Ståhl, S. (2011) Affinity recovery of eight HER2-binding affibody variants using an anti-idiotypic affibody molecule as capture ligand. *Protein Expression Purif. 76*, 127−135.
(60) Ekblad, T., Tolmachev, V., Orlova, A., Lendel, C., Abrahmsén, L., and Karlström, A. E. (2009) Synthesis and chemoselective intramolecular crosslinking of a HER2-binding affibody. *Biopolymers 92*, 116−123.
(61) Orlova, A., Tran, T., Widström, C., Engfeldt, T., Eriksson Karlström, A., and Tolmachev, V. (2007) Pre-clinical evaluation of [111In]-benzyl-DOTA-Z(HER2:342), a potential agent for imaging of HER2 expression in malignant tumors. *Int. J. Mol. Med. 20*, 397−404.
(62) Honovar, H., Westerlund, K., Altai, M., Sandström, M., Orlova, A., Tolmachev, V., and Eriksson Karlström, A. (2015) Feasibility of Affibody Molecule-Based PNA-Mediated Radionuclide Pretargeting, unpublished results.
(63) Kobashigawa, Y., Kumeta, H., Ogura, K., and Inagaki, F. (2009) Attachment of an NMR-invisible solubility enhancement tag using a sortase-mediated protein ligation method. *J. Biomol. NMR 43*, 145−150.
(64) Wållberg, H., Grafström, J., Cheng, Q., Lu, L., Martinsson Ahlzén, H. S., Samén, E., Thorell, J. O., Johansson, K., Dunås, F., Olofsson, M. H., et al. (2012) HER2-positive tumors imaged within 1 h using a site-specifically 11C-labeled Sel-tagged affibody molecule. *J. Nucl. Med. 53*, 1446−1453.
(65) Schmid, F. (2001) Biological Macromolecules: UV-visible Spectrophotometry. In *eLS*, Wiley: Chichester, U.K., http://www.els.net, DOI: 10.1038/npg.els.0003142.

DOI: 10.1021/acs.bioconjchem.5b00292
Bioconjugate Chem. 2015, 26, 1724−1736